

Human Rad52-mediated homology search and annealing occurs by continuous interactions between overlapping nucleoprotein complexes

Eli Rothenberg^a, Jill M. Grimme^b, Maria Spies^{b,c,1}, and Taekjip Ha^{a,b,c,d,1}

^aHoward Hughes Medical Institute and Center for the Physics of Living Cells, Departments of ^bBiochemistry and ^dPhysics, and ^cCenter for Biophysics and Computational Biology, University of Illinois at Urbana-Champaign, Urbana, IL 61801

Edited by James E. Haber, Rosenstiel Center, Waltham, MA, and accepted by the Editorial Board October 29, 2008 (received for review October 14, 2008)

The Rad52 protein has critical functions in distinct pathways of the homology-directed DNA repair, one of which is to promote the annealing of complementary strands of DNA. Both yeast and human Rad52 proteins organize into ring-shaped oligomers with the predominant form being a heptamer. Despite the wealth of information obtained in previous investigations, how Rad52 mediates homology search and annealing remains unclear. Here, we developed single-molecule fluorescence resonance energy transfer approaches to probe hRad52-mediated DNA annealing events in real time. We found that annealing proceeds in successive steps involving rearrangements of the ssDNA-hRad52 complex. Moreover, after initial pairing, further search for extended homology occurs without dissociation. This search process is driven by an interaction between 2 overlapping nucleoprotein complexes. In light of these observations we propose a model for hRad52-mediated DNA annealing where ssDNA release and dsDNA zippering are coordinated through successive rearrangement of overlapping nucleoprotein complexes.

DNA recombination | DNA repair | fluorescence microscopy | FRET | single-molecule

The Rad52 protein belongs to a ubiquitous group of recombination mediator proteins whose function is essential for homologous recombination (HR), homology directed DNA repair, and rescue of collapsed replication forks, serving as a key player in the maintenance of genomic integrity (1–4). All characterized Rad52 proteins facilitate annealing of complementary DNA strands. Moreover, the annealing occurs even in the presence of single-strand binding protein RPA (1, 5–9). This function is critical during several important steps in the recombinational repair, including the second end capture, and the postinvasion ssDNA annealing within the D loop, and the synthesis-dependent strand annealing (7, 10). Although the Rad52 mediator activity in mammalian cells overlaps with functions of other recombinational mediators (11–13), deciphering its molecular mechanism will provide insights into molecular basis of the cellular mechanisms responsible for accurate DNA repair.

Cellular DNA transactions that require annealing of the 2 complementary DNA strands are conserved throughout biology. Consequently, all living organisms possess the ssDNA annealing proteins (14). Many of these proteins are of a different origin and are functional rather than structural homologues. Among them bacterial RecO (15) and invertebrate BRCA2 homologues [such as *Ustilago maydis* Brh2 (13)] were shown to facilitate annealing of ssDNA coated with their cognate ssDNA binding proteins. In contrast, Rad52 paralogue in budding yeast, Rad59 protein fails to facilitate annealing of ssDNA-RPA complexes, but can efficiently anneal naked DNA (16). Recent discovery that a bacteriophage Sak protein is both functional and structural homologue of eukaryotic Rad52 protein suggests the importance of not only annealing per se, but also of the mechanism by which the annealing proceeds (17).

Loading of recombinase proteins during double-strand break repair is another function of Rad52 that is conserved in all

organisms with dsDNA genome. Mediator proteins that possess this function include bacteriophage UvsY protein (18), bacterial RecBCD and RecFOR proteins (19), multiple yeast (1) and mammalian (20) Rad51 paralogues, Rad54 protein (21), and BRCA2 tumor suppression protein (12).

Yeast Rad52 protein has been extensively studied by using both genetic and biochemical approaches (1) because of its essential role in HR and DNA repair. The in vitro analysis of Rad52 annealing activity was extended to the human homologue as well (9, 22–29). Rad52 forms oligomeric ring-shaped structures with hRad52 primarily forming a heptamer (22, 23, 29, 30). High-resolution structures were obtained for the conserved ssDNA annealing domain of hRad52 (24, 25). ssDNA was proposed to bind in the deep groove running around the outer surface of the hRad52 ring mainly by using contacts with the backbone (23–25, 27, 31). Based on the hRad52 structures, an annealing mechanism was proposed where homology is probed 4 nt at a time when the 2 Rad52 oligomers containing ssDNA in the DNA-binding groove transiently come in contact (25). It was unclear, however, whether the 2 Rad52-ssDNA complexes remain associated during the search for complementary regions of sufficient lengths or whether the complexes dissociate after each unsuccessful encounter.

Here, we developed single-molecule fluorescence resonance energy transfer (smFRET) approaches (32–34) to probe hRad52-mediated DNA annealing events in real time. By visualizing individual reactions starting from the initial pairing, we found that annealing proceeds via sequential rearrangements of the ssDNA-hRad52 complex. If the initial pairing does not yield sufficiently stable region that prevails over spontaneous denaturation of the paired strands, further search of longer homology can occur without dissociation of the 2 nucleoprotein complexes. Furthermore, the interaction between 2 nucleoprotein complexes is transient and tends toward a maximal overlap between the 2 complexes. This type of interaction suggests coordination between ssDNA release from hRad52 and dsDNA formation that needs to be repeated multiple times during the annealing processes.

Results and Discussion

Experimental Assay. To probe hRad52 DNA annealing activity, we used smFRET assays based on total internal reflection microscopy which allows simultaneous observation of dozens of annealing reactions. The acceptor (Cy5)-labeled ssDNA strands (target) were tethered to the flow chamber's surface and their complementary donor

Author contributions: E.R. designed research; E.R. performed research; E.R., J.M.G., and M.S. contributed new reagents/analytic tools; E.R. analyzed data; and E.R., M.S., and T.H. wrote the paper.

The authors declare no conflict of interest.

This article is a PNAS Direct Submission. J.E.H. is a guest editor invited by the Editorial Board.

¹To whom correspondence may be addressed. E-mail: mspies@life.uiuc.edu or tjha@uiuc.edu.

This article contains supporting information online at www.pnas.org/cgi/content/full/0810317106/DCSupplemental.

© 2008 by The National Academy of Sciences of the USA

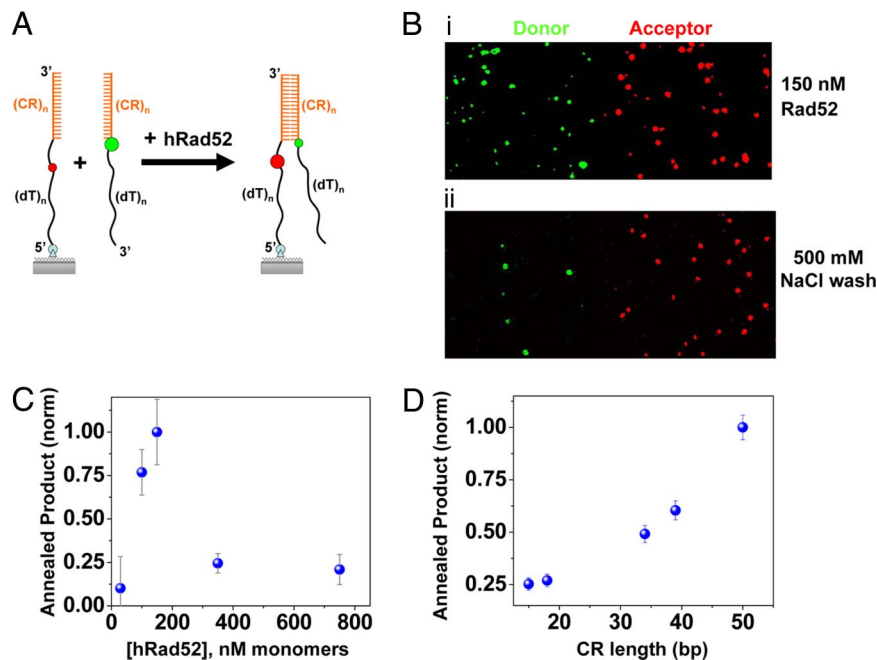


Fig. 1. Single-molecule visualization of hRad52-mediated DNA annealing. (A) Schematic representation of the experimental design and DNA substrates used to investigate length dependence of hRad52-mediated annealing. Red and green circles represent the fluorescence Cy5 and Cy3 dyes, respectively. Relative size of each circle depicts the expected fluorescence of the respective dye. $(CR)_n$ shows the varied complementary region, where n designates the length in nucleotides; $(dT)_n$ represents poly(dT) tails of n nucleotides. (B) Fluorescence images of single-donor molecules (green spots) and corresponding acceptor molecules (red spots) for the substrate with a CR of 18 bp. (i) Annealing in the presence of 150 nM hRad52. (ii) Signal remains after a 500 mM NaCl wash and protein removal, confirming the formation a stable product in the absence of hRad52. (C) The extent of annealing reaction after 5 min (see *Materials and Methods*), normalized to maximum product yield, as a function of hRad52 concentration, showing an increase and subsequent inhibition. Measurements were made after high-salt wash (error bars represent standard error). (D) Length dependence of annealing yield of annealed product (dots) as a function of CR (error bars represent standard error).

(Cy3)-labeled strands (probe) were added together with hRad52. In this scheme no signal is produced unless a complex is formed between the incoming probe strand and the immobilized target strand.

We used the DNA substrates illustrated in Fig. 1A, with complementary regions designed to form stable duplexes at room temperature. The proximity (≈ 7 nt) of the FRET pair in the annealed product resulted in high FRET efficiency and strong acceptor signal. Fig. 1B shows fluorescence images of annealed dsDNA, where the donor and corresponding acceptor spots are on the left and right sides, respectively. The reaction was carried out in the presence of 150 nM hRad52 (Fig. 1Bi) followed by protein removal (Fig. 1Bii) to verify formation of the stable duplex (*Materials and Methods*). We measured the annealing yield as a function of hRad52 concentration at a constant (200 pM) ssDNA concentration (Fig. 1C). A concentration of 150 nM hRad52 was found to be optimal and used for all experiments below. Several control experiments were conducted to verify that our assays appropriately probe the annealing activity of hRad52. No spontaneous annealing occurred under our experimental conditions; the ssDNA concentrations used and lack of salt in the buffer [*Materials and Methods*, [supporting information \(SI\) Fig. S1](#)]. Furthermore, hRad52 does not promote complex formation between 2 strands of ssDNA having no homology (Fig. S1). Finally, we confirmed that efficient annealing activity necessitates both ssDNA strands to be in complex with hRad52 (Fig. S1; J.M.G. and M.S., unpublished work).

Dependence on the Length of the Complementary Regions. Next, we investigated how the length of the complementary region (CR) influences the hRad52-mediated annealing reaction. Five different substrates were used (Fig. 1A) with a comparable total length but different lengths of CR (15, 18, 34, 39, and 50 bp). The real-time hybridization events during the first 2 minutes of data acquisition after addition of the probe strand and hRad52 were counted and showed an increase with increasing CR length (Fig. 1D). This experiment effectively measures the initial rate of homology recognition and shows that a longer CR increases the probability of a productive collision and initial base pairing (3).

Individual annealing traces showed a sudden increase in fluorescence from the background level marking the moment when an incoming donor-labeled ssDNA-hRad52 complex in solution binds its acceptor-labeled target on the surface (Fig. 2A). The subsequent

annealing reaction results in an acceptor signal increase accompanied by a donor signal decrease as the FRET pair is brought closer. The majority of traces showed a distinct initial plateau with a low FRET value before the signal transitioned to a high FRET value (Fig. 2Ai and Aii), but some molecules showed no delay (Fig. 2Aiii). Delay intervals ranged from tens of milliseconds to a few seconds, much too long to stem from annealing of the free DNA strands. The fraction of complexes that spent at least the indicated time before reaching the final high FRET state is plotted versus time for each CR length (Fig. 2B). Because the average delay time between initial pairing and complete annealing increases for longer CRs, we argue that annealing proceeds via multiple steps with the number of steps increasing with increasing CR. Once a limited homology is identified, further annealing and lengthening of dsDNA necessitate release of DNA from the hRad52 ring, because formation of the double helix would require twisting the incoming strand around the strand bound by hRad52 within its ssDNA binding groove, which is too narrow to accommodate dsDNA (31).

In this model, assuming that the initial limited homology can form at any point along the CR, the delay time should depend on the initial pairing location so that initial pairing farther from the fluorophores results in a longer delay time. Indeed, a strong correlation was found between the delay time and initial binding FRET value determined from individual molecules (Fig. 2C for CR = 50; Fig. S2). Moreover, the mean rate for reaching a final high FRET value decreases with increase in CR length, signifying the increase in the necessary number of annealing steps (Fig. 2D).

Transition Between Annealing Configurations Without Dissociation.

To further probe the interactions between 2 nucleoprotein complexes responsible for the annealing reaction, we designed substrates with a CR of only 9 bp ($T_m = 9^\circ\text{C}$). Unlike the substrates used above, a protein-free 9-bp duplex does not form stably under our experimental conditions. The CR was incorporated in the incoming probe strand at 1 of 3 positions: the 3' end (3'-CR), the middle (mid-CR), or the 5' end (5'-CR). The surface-immobilized target strand contained 2 identical CR segments providing 2 pairing configurations with the probe strand, designated as A and B (Fig. 3A). We placed the donor on the probe strand and the acceptor on the target strand in such a way that the A pairing gives a higher FRET value (≈ 0.85) than that of the B pairing (≈ 0.65). Whereas

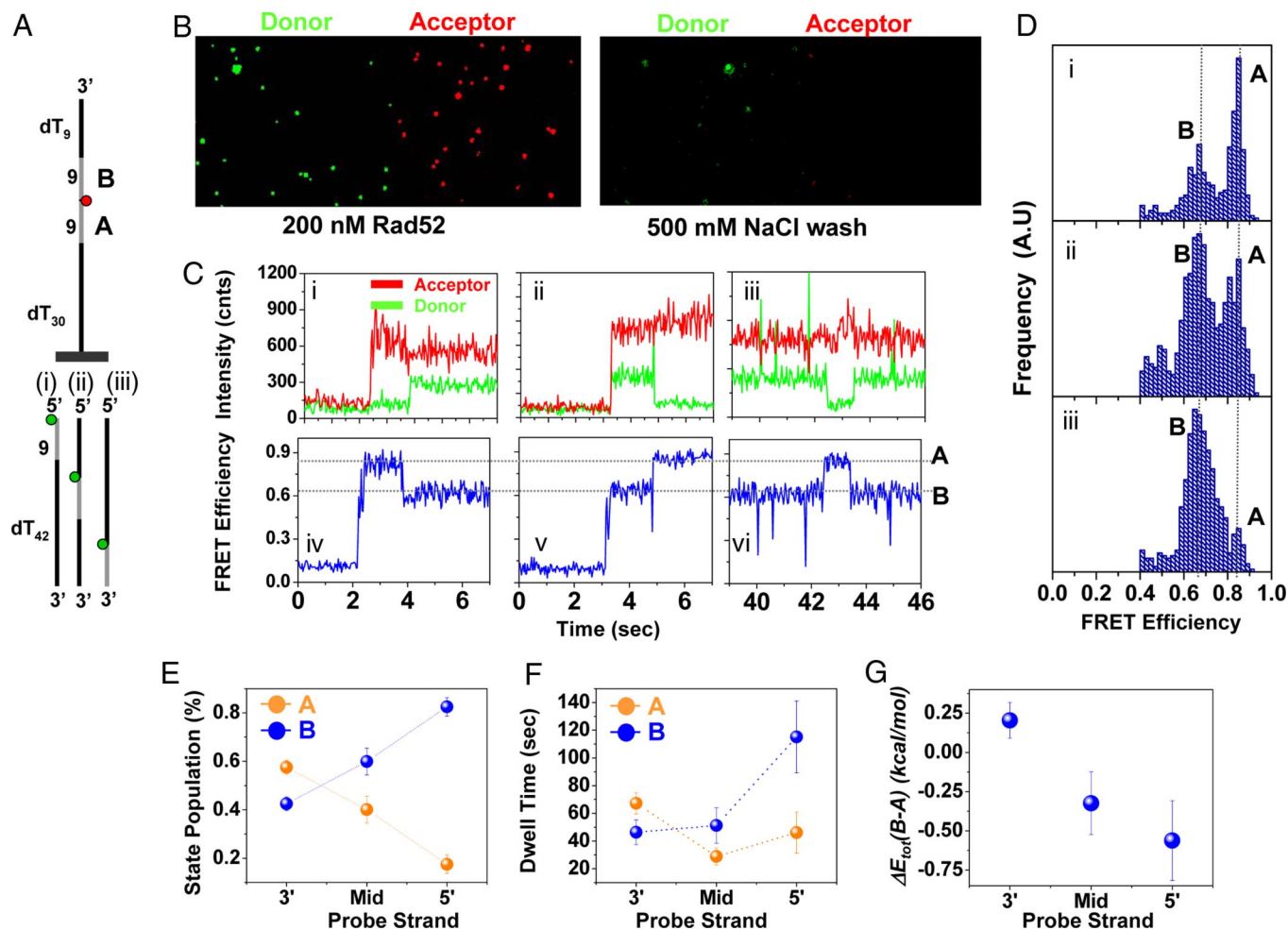


Fig. 3. hRad52 allows hopping between alternative annealing configurations without dissociation. (A) Schematics of the DNA strands used for 9-bp homology. (Top) Surface-tethered, acceptor-labeled strand (target) with 2 identical 9-nt regions. (Bottom *i-iii*) Three donor-labeled strands used (probes), having a 9-nt segment complementary to the 9-nt regions of the target strand in the 3' end (*i*), middle (*ii*), or the 5' end (*iii*). (B) Fluorescence images of single-donor molecules (green spots) and corresponding acceptor molecules (red spots) of the 9-bp annealed product, before (Left) and after (Right) 500 mM NaCl wash, showing that the observed annealed product forms only in the presence of hRad52. (C) Three representative trajectories of single FRET pair donor (green) and its corresponding acceptor (red) intensities (*i-iii*), and their corresponding FRET efficiencies (*iv-vi*, respectively). Panels *i* and *ii* show initial pairing events that are followed by transitions between the 2 states. *iii* shows a transition occurring some time after the initial binding. (D) smFRET histograms showing 2 populations that correspond to hybridization through either of the 2 alternative annealing configurations, A and B, for 3 different probe strands: (*i*) 3'-CR probe, (*ii*) mid-CR probe, and (*iii*) 5'-CR probe. (E) Population of the 2 configurations, A and B, for the 3 different probe strands. Error bars represent standard error from 4 independent experiments each. (F) Average dwell times of A or B for each probe strand. Error bars represent standard error from 4 independent experiments. (G) Energy difference between configurations A and B for each probe strand, as calculated from the dwell time data.

of annealing. This process would result in an increase in ssDNA-hRad52 binding energy (Fig. 5A, cyan curve), but a decrease in the overall energy of the system (red curve).

Mechanism for hRad52-Mediated SSA. Finally, we expand the above model and propose a general mechanism for hRad52-mediated search and annealing (Fig. 5B) that is likely to occur in DSB repair pathway involving single-strand annealing (SSA). hRad52 binds to the resected 3' overhang (9), preventing end degradation (36) and bridging the 2 ends of the break (37). The proximity of the resected ends enables the search for initial homologies through collisions between the 2 nucleoprotein complexes (5, 38–40). The 2 nucleoprotein complexes would then remain in contact while migrating along the complexes to search for the most stable duplex formation (3, 5). The progression of homology search within 2 associated complexes is beneficial for efficiently obtaining a stable duplex configuration while avoiding the need to reinitiate the entire homology search process. Furthermore, such an annealing mechanism may minimize deletion of genetic information that arises due

to erroneous pairing that occurs by chance (41). Our proposed annealing mechanism may also be relevant in D loop formation if a negatively supercoiled DNA transiently forms a single-stranded region to which Rad52 binds.

The present study did not use RPA-coated ssDNA, which should be the physiologically relevant substrate for Rad52-mediated strand annealing reaction. Our bulk solution data predict that although RPA shifts optimal conditions for Rad52 binding and annealing, the overall mechanism of Rad52-mediated annealing does not change in the presence of RPA (J.M.G. and M.S., unpublished work). Future single-molecule studies, for example, with fluorescently labeled RPA molecules, should be able to dissect the interplay between the 2 proteins during the annealing reaction.

Materials and Methods

Materials. All Cy3- or Cy5-labeled, and/or biotin-labeled DNA substrates were purchased from Integrated DNA Technologies (for sequences, see *SI Text*). Isopropyl β -D-1-thiogalactopyranoside (IPTG) and DTT were from Sigma. Complete Protease Inhibitor Mixture Tablets (EDTA-free) were from Roche. All chemicals

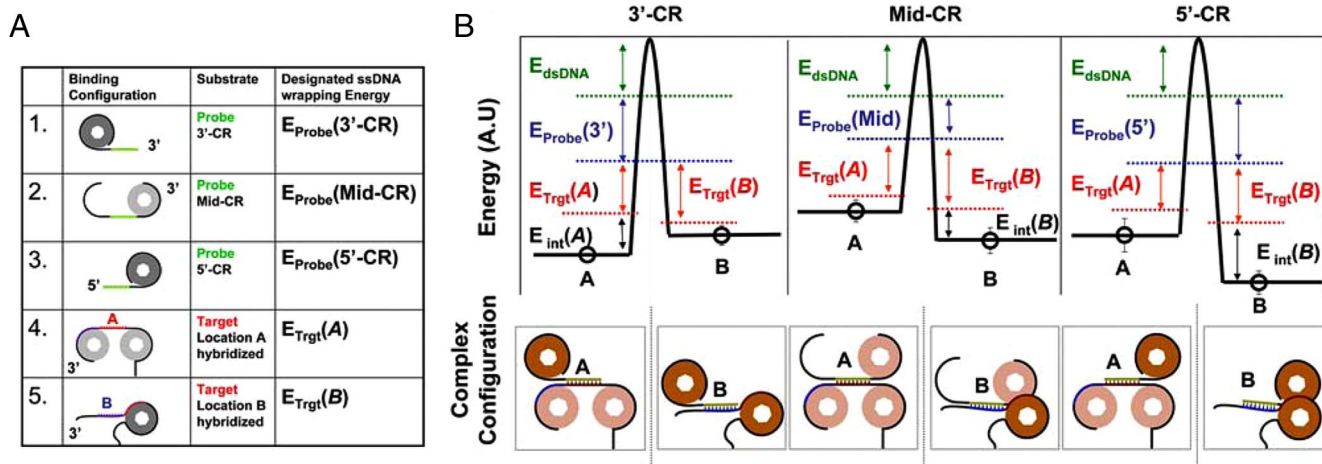


Fig. 4. DNA–hRad52 configurations for maximum complex–complex overlap. (A) Schematic representation of the ssDNA–hRad52 wrapping configurations for the different probes and target, and their designated energies: (1) 3'-CR probe, (2) mid-CR probe, (3) 5'-CR probe, (4) target strand when A is occupied, and (5) target strand when B is occupied. (B) Analysis of the components of the total complex hybridization energy for each configuration of each probe substrate. The parametric total energy in each configuration (open circles) was extracted from the experimental data (see *SI Text*). The contribution for the dsDNA energy (green line) was calculated. The different ssDNA–hRad52 binding and complex–complex interaction energies were estimated with accordance to the configuration as illustrated below (see *SI Text*). The dsDNA energy (green), probe strand–hRad52 binding energy (blue), target strand–hRad52 binding energy (red), the estimated interaction energies between the 2 ssDNA–hRad52 complexes (black).

were reagent grade. pET15b-6HIS-hRad52 plasmid was a generous gift from A. Mazin (Drexel University College of Medicine)

Purification of Human Rad52 Protein. The pET15b-6HIS-hRad52 plasmid was introduced into *Escherichia coli* Rosetta (DE3) pLysS (Novagen). Expression of His₆-Rad52 protein was induced on addition of IPTG (0.25 mM) as described in refs. 6 and 26. His₆-hRad52 protein was purified essentially as described in refs. 6 and 26 with the following column changes: a Ni-charged HiTrap Chelating Sepharose 5-ml column (GE Healthcare), a 5-ml Hi Trap Heparin HP column (GE

Healthcare), and a 6-ml Resource S column (GE Healthcare). Purified His₆-hRad52 protein was stored in 50 mM Tris-HCl, pH 7.5, 1 mM EDTA, 1 mM DTT, and 50% glycerol and stored at -80°C . The hRad52 protein was essentially free of endo- and exonuclease activity. For the DNA binding and annealing assays, hRad52 concentrations given will be expressed as nanomolar monomers unless otherwise indicated.

Single-Molecule FRET Measurements. Single-molecule FRET measurements were performed by using wide-field total-internal-reflection (TIR) fluorescence micro-

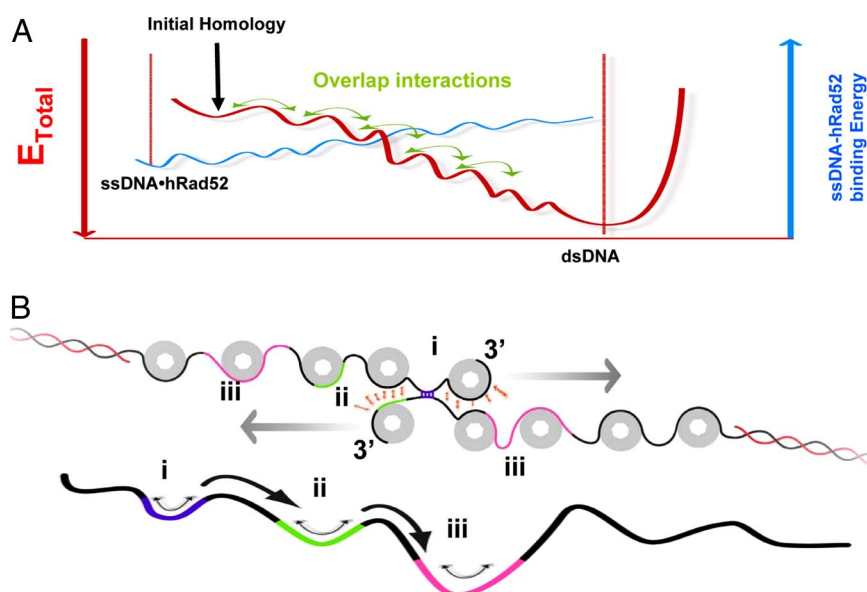


Fig. 5. Successive hRad52-ssDNA release and annealing and general mechanism for homology search and single-strand annealing. (A) Energy landscape illustrating the successive release of ssDNA and dsDNA annealing carried through maximal overlap interaction between complexes. The initial homology is marked, followed by maximal overlap interaction (green arrows), if more homology is found more ssDNA will be released from hRad52 and annealing will progress until the entire region of complementarity is annealed. (B) Mechanism for hRad52-mediated SSA. Diagram representation of 2 interacting ssDNA–hRad52 complexes and schematic energy diagram. After initial unstable pairing with limited homology, marked as homology *i* (purple), corresponding to location *i* (purple) in the energy diagram, the ssDNA–hRad52 will strive for a more stable pairing through the complex–complex overlap interaction (brown arrows), enabling migration to a more substantial homology, marked as homology *ii* (green) corresponding to location *ii* (green) in the energy landscape. If this pairing will not establish a stable configuration, homology search will proceed driven by mean of maximum overlap complex–complex interaction until a stable pairing with sufficient homology is obtained (such as in position *iii*, magenta).

scope. TIR excitation was done either by using a prism, or through an oil-immersion objective (Olympus UplanSAPo 100× numerical aperture 1.4). Images were acquired with a 30-ms time resolution by using an electron-multiplying charge-coupled device (CCD) camera (iXon DV 887-BI, Andor Technology) and a homemade C++ program. FRET values were calculated as the ratio between the acceptor intensity and the sum of the intensities of the donor and acceptor, corrected for filter leakage (42, 43).

A quartz slide was coated with polyethylene glycol (PEG), with 1–2% (wt/wt) of biotin-PEG. Surface integrity and nonspecific binding were measured by separately adding Cy3-labeled DNA (1 nM), and DNA with 200 nM hRad52. Neutravidin was added as described in refs. 42 and 43, followed by immobilizing biotinylated, Cy5-labeled target DNA strand (300 pM DNA). At least a 100-fold reduced number of fluorescence spots were observed on direct excitation of Cy5 by using 632-nm laser when neutravidin was not added beforehand. All measurements were performed at room temperature in a buffer solution: 30 mM Tris-acetate and 1 mM DTT, pH 8.5. Buffer also contained an oxygen scavenger system (0.1 mg/ml glucose oxidase, 0.02 mg/ml catalase, 1% β -mercaptoethanol, and 0.4% (wt/wt) β -D-glucose) and Trolox to eliminate single-molecule blinking events (44).

Single-Molecule hRad52 Mediated Annealing Reaction. The reaction buffer contained no added salt, so that a spontaneous protein-free annealing reaction did not occur even at higher ssDNA concentrations reported here (see controls in Fig. S1). The complementary strands were added in the presence of hRad52 and the reaction was monitored by monitoring an increase in the acceptor signal (Fig. 1B). Because the acceptor (Cy5) on the surface-tethered strand is not excited by the 532-nm laser excitation efficiently, no signal is observed unless the incoming donor (Cy3)-labeled strand forms a complex with the acceptor strand. To verify dsDNA formation, free ssDNA–hRad52 and hRad52 were removed from the flow chamber after 5 min incubation by washing with the reaction buffer containing no protein. This was followed by a high-salt (500 mM NaCl) buffer wash, which

removed the bound hRad52. The molecules were then imaged again. Presence of a persistent acceptor signal indicated the formation of a stable dsDNA product.

Protein Concentration Dependence. The surface-immobilized strand 48 nt in overall length was composed of biotin at the 5' end of 30 dT and the acceptor Cy5 dye incorporated within the poly(dT) region 7 nt from the start of a random 18-nt sequence at the 3' end. The 48-nt donor-labeled strand consists of a 3' stretch of 30 poly(dT) residues followed by the complementary random 18-nt sequence at the 5' end. The Cy3 dye was incorporated internally to the complementary DNA region. When annealed, the positions of the donor and acceptor fluorophores would result in a high FRET signal. DNA concentrations used were constant for the surface-bound strand (300 pM) and the free donor strand (200 pM). The hRad52 protein concentration was varied from 30 to 750 nM. Data were plotted by using Origin 7 software.

Complementary Length Dependence. The substrates used had varying lengths of complementary regions (15, 18, 34, 39, and 50 bp) with the total lengths of the substrates in the range of 58–78 nt and 48–80 nt for target and probe strands, respectively. For each complementary length pair, DNA concentrations used for donor- and acceptor-labeled strands were 300 pM per oligonucleotide and the hRad52 protein concentration was 200 nM. The acceptor-labeled strand was immobilized to the surface and the donor-labeled strand that had been preincubated with hRad52 protein was added to the reaction chamber by buffer exchange. Data collection was started before addition of the DNA–hRad52 mixture.

ACKNOWLEDGMENTS. We thank Dr. Alexander Mazin (Drexel University) for the plasmid for hRad52 expression. E.R. thanks Hamza Balci and Yuval Ofir for proofreading the manuscript. This work was supported in part by National Institutes of Health Grant GM065367 (to T.H.) and National Science Foundation Physics Frontiers Grant 0822613. E.R. was supported in part by a European Molecular Biology Organization long-term fellowship and by the Howard Hughes Medical Institute. T.H. is an investigator with the Howard Hughes Medical Institute.

- Symington LS (2002) Role of RAD52 epistasis group genes in homologous recombination and double-strand break repair. *Microbiol Mol Biol Rev* 66:630–670.
- Ivanov EL, Sugawara N, Fishman-Lobell J, Haber JE (1996) Genetic requirements for the single-strand annealing pathway of double-strand break repair in *Saccharomyces cerevisiae*. *Genetics* 142:693–704.
- Sugawara N, Ira G, Haber JE (2000) DNA length dependence of the single-strand annealing pathway and the role of *Saccharomyces cerevisiae* RAD59 in double-strand break repair. *Mol Cell Biol* 20:5300–5309.
- Sugawara N, Wang X, Haber JE (2003) In vivo roles of Rad52, Rad54, and Rad55 proteins in Rad51-mediated recombination. *Mol Cell* 12:209–219.
- Mortensen UH, Bendixen C, Sunjevaric I, Rothstein R (1996) DNA strand annealing is promoted by the yeast Rad52 protein. *Proc Natl Acad Sci USA* 93:10729–10734.
- Reddy G, Golub EI, Radding CM (1997) Human Rad52 protein promotes single-strand DNA annealing followed by branch migration. *Mutat Res* 377:53–59.
- Mcllwraith MJ, West SC (2008) DNA repair synthesis facilitates RAD52-mediated second-end capture during DSB repair. *Mol Cell* 29:510–516.
- Barzel A, Kupiec M (2008) Finding a match: How do homologous sequences get together for recombination? *Nat Rev Genet* 9:27–37.
- Van Dyck E, Stasiak AZ, Stasiak A, West SC (2001) Visualization of recombination intermediates produced by RAD52-mediated single-strand annealing. *EMBO Rep* 2:905–909.
- Lao Y, Lee CG, Wold MS (1999) Replication protein A interactions with DNA. 2. Characterization of double-stranded DNA-binding/helix-destabilization activities and the role of the zinc-finger domain in DNA interactions. *Biochemistry* 38:3974–3984.
- de Vries FA, et al. (2007) Schizosaccharomyces pombe Rad22A and Rad22B have similar biochemical properties and form multimeric structures. *Mutat Res* 615:143–152.
- Esashi F, Galkin VE, Yu X, Egelman EH, West SC (2007) Stabilization of RAD51 nucleoprotein filaments by the C-terminal region of BRCA2. *Nat Struct Mol Biol* 14:468–474.
- Mazloum N, Zhou Q, Holloman WK (2007) DNA Binding, annealing, and strand exchange activities of Brh2 protein from *Ustilago maydis*. *Biochemistry* 46:7163–7173.
- Iyer LM, Koonin EV, Aravind L (2002) Classification and evolutionary history of the single-strand annealing proteins, RecT, Redbeta, ERF and RAD52. *BMC Genomics* 3:8.
- Kantake N, Madiraju MV, Sugiyama T, Kowalczykowski SC (2002) *Escherichia coli* RecO protein anneals ssDNA complexed with its cognate ssDNA-binding protein: A common step in genetic recombination. *Proc Natl Acad Sci USA* 99:15327–15332.
- Sugiyama T, Kantake N, Wu Y, Kowalczykowski SC (2006) Rad52-mediated DNA annealing after Rad51-mediated DNA strand exchange promotes second ssDNA capture. *EMBO J* 25:5539–5548.
- Ploquin M, et al. (2008) Functional and structural basis for a bacteriophage homolog of human RAD52. *Curr Biol* 18:1142–1146.
- Liu J, Bond JP, Morrill SW (2006) Mechanism of presynaptic filament stabilization by the bacteriophage T4 UvsY recombination mediator protein. *Biochemistry* 45:5493–5502.
- Spies M, Kowalczykowski SC (2005) Homologous recombination by RecBCD and RecF pathways. *The Bacterial Chromosome* (ASM Press, Washington, DC), pp 389–403.
- Thompson LH, Schild D (2001) Homologous recombinational repair of DNA ensures mammalian chromosome stability. *Mutat Res* 477:131–153.
- Mazin AV, Alexeev AA, Kowalczykowski SC (2003) A novel function of Rad54 protein. Stabilization of the Rad51 nucleoprotein filament. *J Biol Chem* 278:14029–14036.
- Shinohara A, Shinohara M, Ohta T, Matsuda S, Ogawa T (1998) Rad52 forms ring structures and co-operates with RPA in single-strand DNA annealing. *Genes Cells* 3:145–156.
- Van Dyck E, Hajibagheri NM, Stasiak A, West SC (1998) Visualisation of human rad52 protein and its complexes with hRad51 and DNA. *J Mol Biol* 284:1027–1038.
- Kagawa W, et al. (2002) Crystal structure of the homologous-pairing domain from the human Rad52 recombinase in the undecameric form. *Mol Cell* 10:359–371.
- Singleton MR, Wentzell LM, Liu Y, West SC, Wigley DB (2002) Structure of the single-strand annealing domain of human RAD52 protein. *Proc Natl Acad Sci USA* 99:13492–13497.
- Benson FE, Baumann P, West SC (1998) Synergistic actions of Rad51 and Rad52 in recombination and DNA repair. *Nature* 391:401–404.
- Lloyd JA, McGrew DA, Knight KL (2005) Identification of residues important for DNA binding in the full-length human Rad52 protein. *J Mol Biol* 345:239–249.
- Parsons CA, Baumann P, Van Dyck E, West SC (2000) Precise binding of single-stranded DNA termini by human RAD52 protein. *EMBO J* 19:4175–4181.
- Stasiak AZ, et al. (2000) The human Rad52 protein exists as a heptameric ring. *Curr Biol* 10:337–340.
- Lloyd JA, Forget AL, Knight KL (2002) Correlation of biochemical properties with the oligomeric state of human rad52 protein. *J Biol Chem* 277:46172–46178.
- Kagawa W, et al. (2008) Identification of a second DNA binding site in the human Rad52 protein. *J Biol Chem* 283:24264–24273.
- Ha T, et al. (1996) Probing the interaction between two single molecules: Fluorescence resonance energy transfer between a single donor and a single acceptor. *Proc Natl Acad Sci USA* 93:6264–6268.
- Zeng Y, et al. (2007) Probing nucleation, reverse annealing, and chaperone function along the reaction path of HIV-1 single-strand transfer. *Proc Natl Acad Sci USA* 104:12651–12656.
- Zhuang XW, et al. (2000) A single-molecule study of RNA catalysis and folding. *Science* 288:2048–2051.
- Ranatunga W, et al. (2001) Human RAD52 exhibits two modes of self-association. *J Biol Chem* 276:15876–15880.
- Aylon Y, Liefshitz B, Bitan-Banin G, Kupiec M (2003) Molecular dissection of mitotic recombination in the yeast *Saccharomyces cerevisiae*. *Mol Cell Biol* 23:1403–1417.
- Kaye JA, et al. (2004) DNA breaks promote genomic instability by impeding proper chromosome segregation. *Curr Biol* 14:2096–2106.
- Soutoglou E, et al. (2007) Positional stability of single double-strand breaks in mammalian cells. *Nat Cell Biol* 9:675–682.
- Storici F, Snipe JR, Chan GK, Gordenin DA, Resnick MA (2006) Conservative repair of a chromosomal double-strand break by single-strand DNA through two steps of annealing. *Mol Cell Biol* 26:7645–7657.
- Haviv-Chesner A, Kobayashi Y, Gabriel A, Kupiec M (2007) Capture of linear fragments at a double-strand break in yeast. *Nucleic Acids Res* 35:5192–5202.
- Richardson C, Stark JM, Ommundsen M, Jasim M (2004) Rad51 overexpression promotes alternative double-strand break repair pathways and genome instability. *Oncogene* 23:546–553.
- Ha T (2001) Single-molecule fluorescence resonance energy transfer. *Methods* 25:78–86.
- Rasnik I, Myong S, Cheng W, Lohman TM, Ha T (2004) DNA-binding orientation and domain conformation of the *E. coli* Rep helicase monomer bound to a partial duplex junction: Single-molecule studies of fluorescently labeled enzymes. *J Mol Biol* 336:395–408.
- Rasnik I, McKinney SA, Ha T (2006) Nonblinking and longlasting single-molecule fluorescence imaging. *Nature Methods* 3:891–893.